Nucleon-nucleon cross sections in dense nuclear matter

H. F. Zhang,[1] Z. H. Li,[2] U. Lombardo,[2,3] P. Y. Luo,[4] F. Sammarruca,[5] and W. Zuo[4]
[1]*School of Nuclear Science and Technology, Lanzhou University, Lanzhou 730000, People's Republic of China*
[2]*INFN-LNS, Via S. Sofia 64, I-95123 Catania, Italy*
[3]*Dipartimento di Fisica e Astronomia, Via A. Doria 6, I-95123 Catania, Italy*
[4]*Institute of Modern Physics, Chinese Academy of Science, Lanzhou 730000, People's Republic of China*
[5]*Physics Department, University of Idaho, Moscow, Idaho 83844-0903, USA*
(Received 1 August 2007; published 12 November 2007)

We present microscopic calculations of cross sections for scattering of identical and nonidentical nucleons in symmetric nuclear matter at various densities, using the Brueckner-Hartree-Fock approximation scheme with the Argonne v_{14} potential including the contribution of microscopic three-body forces. We investigate separately the effects of three-body forces on the effective mass and on the scattering amplitude. In the present calculation, the rearrangement contribution of the three-body force is considered, which reduces the neutron and proton effective mass and suppresses the magnitude of the cross section. The presence of "Z diagrams" in the three-body force enables us to make a comparison with the medium effects on the nucleon-nucleon cross sections obtained with the Dirac-Brueckner-Hartree-Fock approximation.

DOI: 10.1103/PhysRevC.76.054001 PACS number(s): 21.65.+f, 21.30.Fe, 24.10.Cn, 25.75.−q

I. INTRODUCTION

Heavy-ion collisions (HICs) are theoretically described by transport-model simulations whose input data are the in-medium cross sections and the nuclear mean field [1]. Being intimately related to each other through the nuclear matter equation of state (EOS), they must be consistently determined. Microscopic approaches to the EOS, which are based on the bare nucleon-nucleon (NN) force, exhibit the unique advantage of deriving both inputs on the same footing and thus allow for consistency in the approximations adopted at each level. Concerning in-medium NN cross sections, which is the focal point of this study, several calculations exist in the literature based on Brueckner theory [2,3], Dirac-Brueckner (DB) theory [4,5], and variational approaches [6].

In Brueckner theory, the G matrix plays the role of the in-medium scattering amplitude, with medium effects being introduced through the mean field and Pauli blocking. In the zero density limit, the G matrix reduces to the T matrix, and the Brueckner-Bethe-Goldstone (BBG) equation to the Lippmann-Schwinger equation.

During the impact phase between two heavy ions from high-energy central collisions, the nucleon density can reach values up to twice the saturation density. Under these conditions, although dispersion and Pauli blocking effects play a significant role, medium modifications induced by virtual excitations of $N\bar{N}$ states and nucleon resonances [$\Delta(1232)$ or Roper $N^*(1440)$] are expected to become increasingly important. It is well known that these effects can be described in terms of three-body forces (3BFs) [7–9].

Beyond the scattering amplitude, NN collisions in nuclear matter are also driven by kinematic degrees of freedom, i.e., entrance flow and density of states in the exit channel. Both are related to the nucleon effective mass, which, in turn, is related to the self-energy. The latter is modified by a 3BF, which also generates quite large rearrangement terms [10], leading, in turn, to a large reduction of the effective mass. Thus one can expect that 3BFs might have a strong influence on the in-medium cross sections, as they depend quadratically on the effective mass.

Among the three-body forces included in the calculations are the so-called Z diagrams, corresponding to virtual nucleon-antinucleon excitations. Already, earlier studies [11,12] have argued that these provide the main relativistic effect missing from conventional Brueckner theory. Moreover, it is claimed that the relativistic Dirac-Brueckner-Hartree-Fock (DBHF) approach takes those Z graphs into account [11]. The main argument is that a Dirac spinor containing an effective mass can be expanded in a complete set of free-space spinors and thus effectively includes antiparticle contributions. On the other hand, an in-depth quantitative analysis of this "equivalence" has not been done, to the best of our knowledge. It is our plan to perform such an analysis and shed more light on the relation between the two methods. With that in mind, following a systematic presentation of new in-medium cross section results (obtained with the 3BF), we will compare them with those from recent DBHF calculations.

In Sec. II, we review the BHF approximation with the 3BF and the relation with the DBHF approximation; the formalism of the in-medium cross section in the two approximations is developed in Sec. III. In Sec. IV, results are discussed for scattering between identical nucleons as well as neutrons and protons. Special attention is devoted to the comparison of the BHF and DBHF predictions for the cross section. Our conclusions are drawn in Sec. V.

II. FORMALISM

A. Review of nonrelativistic Brueckner theory with 3BF

In the context of Brueckner theory, the role of the amplitude for scattering of two nucleons embedded in a nuclear environment is played by the G matrix, which satisfies the

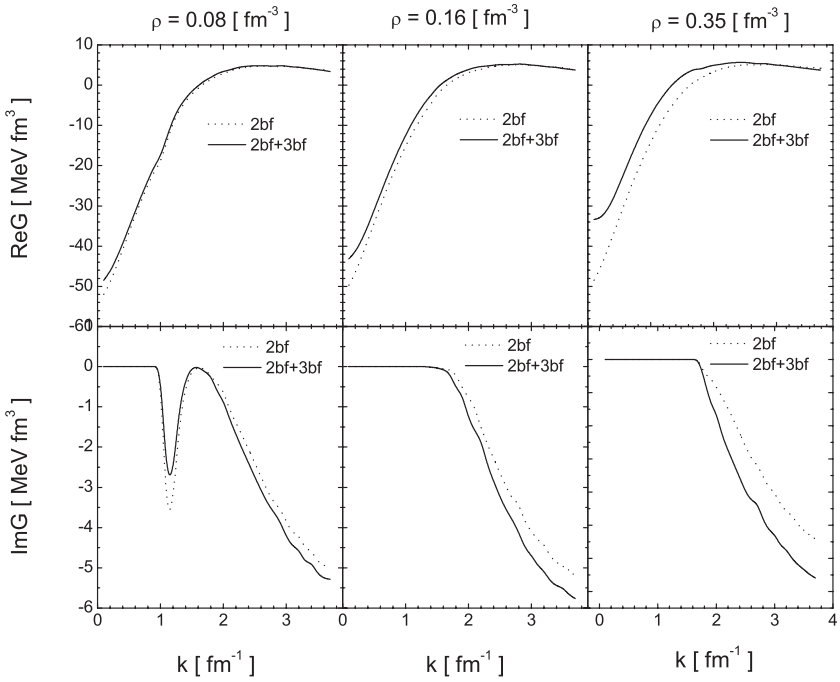

FIG. 1. Real and imaginary parts of the $^1S_0$ components of the G matrix at different densities with (solid lines) and without (dotted lines) the contribution of 3BFs to the mean field.

Brueckner-Bethe-Goldstone (BBG) equation [13,14]:

$$G(\rho,\omega) = v_{NN} + v_{NN}\sum_{k_1k_2}\frac{|k_1k_2\rangle Q\langle k_1k_2|}{\omega-\epsilon(k_1)-\epsilon(k_2)}G(\rho,\omega), \quad (1)$$

where ω is the starting energy, and Q is the Pauli operator, which prevents the two nucleons from being scattered into occupied states. $\epsilon(k)$ is the single-particle energy given by $\epsilon(k) = \hbar^2k^2/(2m) + U(k)$, with $U(k)$ the single-particle potential. For the latter, we adopt the so-called continuous choice [13,14]; i.e., for momenta k below and above the Fermi surface, we define

$$U(k) = \mathrm{Re}\sum_{k'\leqslant k_F}\langle kk'|G[\rho;e(k)+e(k')]|kk'\rangle_a, \quad (2)$$

where the subscript a denotes antisymmetrization of the matrix element. Because of the occurrence of $U(k)$ in Eqs. (1) and (2), the latter forms a coupled system of equations that must be solved in a self-consistent way. In the limit of zero density, the BBG equation reduces to the Lippmann-Schwinger equation, and the G matrix to the T matrix.

For scattering between two particles in the presence of a medium, in addition to the two-body bare interaction, 3BFs must be considered to take into account virtual excitations of nucleon resonances and $N\bar{N}$ pairs [7]. The 3BF adopted in the present calculation is based on the meson-exchange current model, and it is described in full detail in Ref. [9]. To be applied to the Brueckner approach, the 3BF has been converted into an effective two-body force by averaging out the third particle weighted on the two-body correlation function, i.e.,

$$\langle\vec{r}_1\vec{r}_2|V_3^{\tau_1\tau_2}|\vec{r}_1'\vec{r}_2'\rangle = \frac{1}{4}\sum_{\tau_3}\sum_{\sigma_3}\sum_{n}\int \mathrm{d}\vec{r}_3\mathrm{d}\vec{r}_3'\phi_n^* \times(\tau_3\vec{r}_3')(1-\eta_{\tau_1,\tau_3}(r_{13}'))(1-\eta_{\tau_2,\tau_3}(r_{23}')) \times W_3(\vec{r}_1'\vec{r}_2'\vec{r}_3'|\vec{r}_1\vec{r}_2\vec{r}_3)\phi_n(\tau_3r_3) \times(1-\eta_{\tau_1,\tau_3}(r_{13}))(1-\eta_{\tau_2,\tau_3}(r_{23})). \quad (3)$$

The function $\eta_{\tau_1\tau_2}(r)$ is the spin and momentum average of the defect function, of which only the most important partial wave components have been included, i.e., the $^1S_0$ and $^3S_1 - 3D_1$ partial waves.

The transformation of the 3BF to an effective 2BF entails a self-consistent coupling between the 3BF and Brueckner procedures for solving the Brueckner-Bethe-Goldstone equations. One begins by calculating the correlation function with the 2BF only and then builds up the effective 3BF, which, in turn, is added to the 2BF. The correlation function is recalculated, and the whole procedure is repeated until convergence is reached. Terms up to $l_{\max} = 6$ have been retained in the partial wave expansion of the full interaction.

In Fig. 1, the G matrix in the $^1S_0$ channel is plotted. While 3BFs are negligible at low density, they start to be noticeable at saturation density and become more and more effective as density increases. We see that the real part of the G matrix is reduced due to Pauli blocking and dispersive effects. The imaginary part, which is related to the particle-hole excitations, becomes larger because of the 3BF enhancement of the ground state correlations. As is well known, the G matrix shows a spurious singular behavior around the Fermi energy due to the missing pairing correlations from the BHF approximation. In fact, when the latter are included in the calculations, the singularity disappears [15]. Since the singularity in the real part of the G matrix is very narrow, it was easily eliminated by hand. The same was done for the imaginary part at high density.

In addition to the in-medium scattering amplitude, the NN cross section also depends on the density of states, which is given by the inverse derivative of the single-particle energy

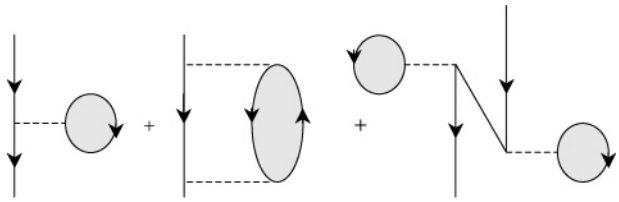

FIG. 2. Self-energy diagrams: BHF term (left), correlation term (middle), and Z diagram (right). The latter is one of the 3BF contributions included in the calculations.

with respect to momentum. In vacuum, it is determined by the kinetic energy, and it turns out to be proportional to the bare mass m. In the medium, the additional contribution from the self-energy can be reasonably approximated by replacing the bare mass with the effective mass, which is given by

$$\frac{m^*(k)}{m} = \frac{k}{m}\left(\frac{d\epsilon(k)}{dk}\right)^{-1}. \tag{4}$$

In the BHF approximation with the 3BF, the self-energy contains three terms,

$$\Sigma(k) = \Sigma_{\rm BHF}(k) + \Sigma_{\rm corr}(k) + \Sigma_{\rm 3BF}(k), \tag{5}$$

where the first term is the mean field with inert core, the second term accounts for the core polarization, and the third term corresponds to the rearrangement contribution associated with the density dependence of the effective 3BF [10]. The corresponding diagrams are displayed in Fig. 2.

In Fig. 3, the effective mass is shown as a function of the momentum at three densities. The effective mass becomes substantially smaller with the inclusion of the 3BF, an effect which will impact the in-medium cross sections through the level densities in the entrance and exit channels, along with the 3BF enhancement of the repulsive components in the effective interaction.

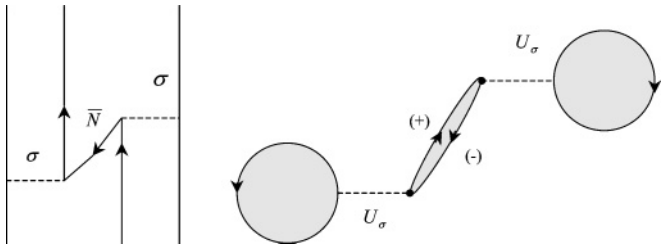

FIG. 4. Z diagram (left) and its contribution to the nuclear matter energy (right). Upward/downward lines represent positive/negative energy states.

B. BHF with 3BF vs DBHF approach

The relationship between nonrelativistic Brueckner theory and the relativistic DBHF theory was discussed already over two decades ago [11,12]. The single-particle spectrum in the DBHF theory includes states of positive and negative energy (Dirac sea) which are coupled by the interaction. The latter can be incorporated in the nonrelativistic Brueckner theory by introducing a 3BF, where three particles interact via nucleon-antinucleon virtual excitations, as shown in Fig. 4. Their contribution to the BHF energy turns out to be strongly density dependent and provides a very efficient saturation mechanism.

Here, we concentrate on reviewing some of the basic concepts leading to the conclusion that relativistic effects (to lowest order) tie in with the virtual excitation of pair terms at the level of the nucleon self-energy. Relativistic Brueckner-Hartree-Fock calculations such as those reported in Refs. [16–18] include explicit negative energy states in the intermediate two-particle propagator as well, whereas we apply the Thompson reduction to our in-medium two-particle propagator, consistent with the free-space equation used with the relativistic Bonn potential [19].

One starts with the free Dirac wave function, which has the form

$$u_+(\mathbf{p},\lambda) = \sqrt{\frac{E_p+m}{2m}}\begin{pmatrix}\chi_\lambda \\ \frac{\sigma\cdot\mathbf{p}}{E_p+m}\chi_\lambda\end{pmatrix} \tag{6}$$

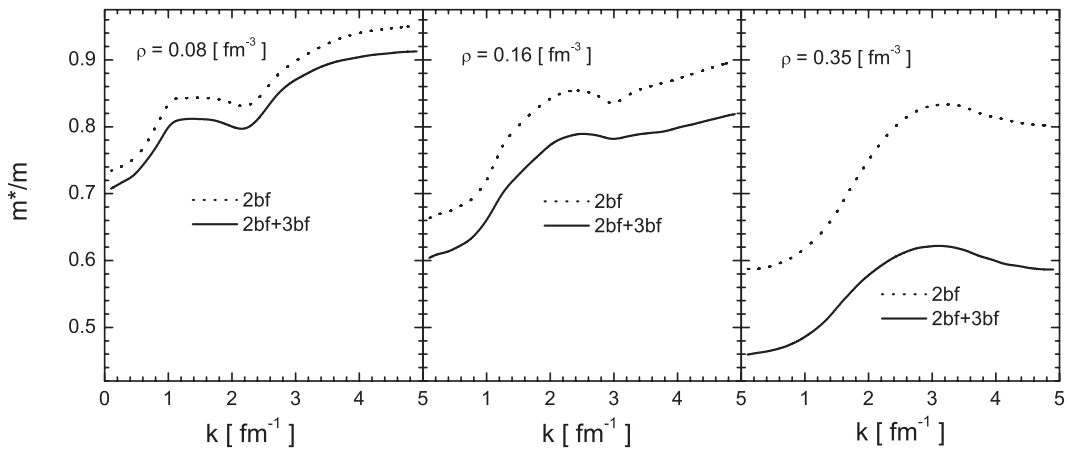

FIG. 3. Momentum dependence of the nucleon effective mass m^*/m in symmetric nuclear matter at three densities, in the presence and absence of the 3BF effect.

for positive energy, and

$$u_{-}(\mathbf{p},\lambda)=\sqrt{\frac{E_p+m}{2m}}\begin{pmatrix}\frac{-\sigma\cdot\mathbf{p}}{E_p+m}\phi_\lambda\\ \phi_\lambda\end{pmatrix} \tag{7}$$

for negative energy. In these equations, χ and ϕ are Pauli spinors, and $E_p=\sqrt{m^2+\mathbf{p}^2}$.

In nuclear matter, the familiar one-body equation in the mean field approximation is written as

$$[\alpha\cdot\mathbf{p}+\beta(m+U_S)-(\epsilon_p-U_V)]u(\mathbf{p},\lambda)=0, \tag{8}$$

where $\alpha^k=\gamma^0\gamma^k$, $\beta=\gamma^0$, and $U_{S/V}$ are the scalar/vector components of the nucleon Dirac self-energy. It is then easy to see that the inclusion of U_S and U_V simply amounts to replacing m with $\tilde{m}=m+U_S$ in the free Dirac solutions. Positive and negative energy states can now be connected through the scalar field, which therefore can be identified as the source of the leading relativistic correction to the propagation of positive energy states. The latter is then essentially equivalent to a medium effect and can be interpreted as a three-body force. This is depicted in the left-hand side of Fig. 4, the well-known Z diagram.

From the correction to the positive energy solution, one can estimate the corresponding contribution to the nuclear matter energy (depicted in the right-hand side of Fig. 4). To lowest order in p/m, the relativistic correction to the energy can be approximated by the formula

$$\frac{\Delta E}{A}\approx 4MeV\left[\frac{\rho_B}{\rho_0}\right]^{8/3}, \tag{9}$$

as shown in Refs. [11,12]. A close estimate was derived in Ref. [7], where the role of the scalar U_S field is played by the scalar σ meson. [To avoid confusion, we stress that Eq. (9) is just a crude estimate from earlier works. All models considered here obtain the energy per particle fully self-consistently within their respective frameworks.]

To summarize, in this brief subsection we have reviewed the main arguments linking relativistic corrections with (some) many-body effects. Of course, it must be kept in mind that important differences do exist between the DBHF approximation and the BHF approach with a full 3BF. In the former, relativistic corrections effectively take into account virtual antinucleon excitations in the nucleon self-energy, whereas in the latter other contributions due to virtual nucleon excitations [Δ and $N^*(1440)$ resonances] are also included. The difference between the two approaches can be appreciated by comparing the energy per particle as obtained in the two cases, see Table I. The saturation density and energy are very close to each other, but the EOS from DBHF is much stiffer ($K=259$ MeV) than the one from BHF+3BF ($K=206$ MeV). It is most interesting to observe how the values shown in the last column (where the effect of Z diagrams has been extracted from the full 3BF), are in much better agreement with the DBHF predictions than those from BHF+3BF, especially at the higher densities, where the predictions with 3BF are considerably more attractive. This supports the argument that Z-diagram correlations can be reasonably described in the DBHF approximation. The comparison still deserves additional investigation.

TABLE I. Energy per particle (in MeV) from DBHF [20], BHF with the full 3BF [9], and BHF with just the Z-diagram correlation.

k_F (fm^{-1})	ρ (fm^{-3})	E/A^{DBHF}	$E/A^{\mathrm{BHF+3BF}}$	$E/A^{\mathrm{BHF+Z}}$
0.80	0.0346	−7.178	−5.413	−5.057
0.90	0.0492	−8.883	−7.352	−6.732
1.00	0.0675	−10.68	−9.133	−8.226
1.10	0.0899	−12.51	−10.73	−9.657
1.20	0.1167	−14.21	−13.04	−10.32
1.30	0.1484	−15.55	−14.64	−13.12
1.35	0.1662	−15.97	−15.17	−14.75
1.40	0.1854	−16.14	−15.78	−14.21
1.45	0.2059	−16.00	−16.06	−14.64
1.50	0.2280	−15.43	−16.02	−14.19
1.60	0.2767	−12.43	−14.82	−11.34
1.70	0.3319	−5.424	−11.34	−4.773
1.80	0.3939	7.283	−4.866	5.778
1.90	0.4633	26.50	5.256	22.97
1.95	0.5009	38.56	11.66	32.42
2.00	0.5404	52.16	20.36	49.52
2.05	0.5819	67.24	29.59	63.52

III. IN-MEDIUM CROSS SECTIONS

In the c.m. frame, the nonrelativistic elastic differential cross section for neutron-proton (np) scattering from unpolarized beams is given by

$$\sigma_{np}(\theta)=\frac{m^{*2}}{4\pi^2\hbar^4}\sum_{SS_zS_z'}\left|G^S_{S_zS_z'}(\theta)\right|^2. \tag{10}$$

In the case of collisions between identical particles, i.e., neutron-neutron or proton-proton collisions (hereafter denoted as NN collisions), antisymmetrization requires us to sum up the two scattering amplitudes G(θ) and G($\pi-\theta$) before taking the modulus square:

$$\sigma_{NN}(\theta)=\frac{m^{*2}}{16\pi^2\hbar^4}\sum_{SS_zS_z'}\left|G^S_{S_zS_z'}(\theta)+(-1)^S G^S_{S_zS_z'}(\pi-\theta)\right|^2. \tag{11}$$

The Coulomb force is neglected in this investigation. The G matrix is the on-shell in-medium scattering amplitude, including Pauli blocking and the dispersive effect from the mean field, as shown in the BBG equation (1). The prefactor is the density of states of nuclear matter in the entrance and exit channels. The effective mass comes from the momentum dependence of the mean field (Schrödinger mass) and thus has a different physical origin than the effective mass related to the renormalization of the self-energy due to the scalar field (Dirac mass) [5,21].

The spin components of the G matrix are obtained by summing up angular states as

$$G^S_{S_zS_z'}(\theta)=\sum_{LL'J}Y^{S_z'-S_z}_{L'}(\theta,0)\langle L0,SS_z'|JS_z'\rangle \times\langle L'S_z'-S_z,SS_z|JS_z'\rangle\langle k;L'SJ|G|k;LSJ\rangle, \tag{12}$$

where the brackets are the Clebsch-Gordan coefficients and Y^M_L are the spherical harmonics. Employing the latter

expression, the differential cross section can be explicitly integrated over the solid angle to give the total cross section valid for both like and unlike particles,

$$\sigma_{\rm tot}(E) = \frac{m^{*2}}{16\pi^2\hbar^4}\sum_{SJ}\sum_{L'L} \times [1-(-1)^{S+L+T}]^2 \frac{2J+1}{4\pi}\left|G^{SJ}_{L'L}\right|^2. \quad (13)$$

When operating within a relativistic framework, one uses the expression for the relativistic elastic differential cross section. In units consistent with Eqs. (10)–(13), it reads

$$\sigma(\theta) = \frac{\tilde{m}^4}{4\pi^2\hbar^4\tilde{s}}|\hat{G}(\theta)|^2, \quad (14)$$

where $\tilde{m} = m + U_S$, with U_S the scalar component of the nucleon self-energy, see Eq. (8), and $\tilde{s} = 4(\tilde{m}^2 + \vec{q}^2) = 4\tilde{E}^2$. The relativistic and nonrelativistic amplitudes are related by $\hat{G} = \frac{\tilde{E}}{\tilde{m}}G$, which provides the connection between Eqs. (11) and (14).

Notice that the crucial point in the relativistic Dirac-Brueckner-Hartree-Fock scheme is the presence of $\tilde{m}$ in the nucleon Dirac wave function, which is precisely the effect discussed in Sec. II B.

IV. RESULTS AND DISCUSSION

In-medium NN cross sections have been calculated with various methods and discussed in several papers [3–5,22–26]. Concerning BHF (strictly two-body) approaches, one must keep in mind that the applicability of these predictions is restricted to low density, and therefore the corresponding in-medium cross sections cannot describe the entire evolution of a HIC and other phenomena where high baryon density is involved. Extension of the BHF approximation to include 3BFs permits us to widen its range of applicability up to very high density. Therefore, in-medium cross sections are now revisited through new calculations, emphasizing the role of 3BFs. Since one important component of a 3BF is closely related to $N\bar{N}$ excitations (see comments in Sec. II B), a comparison with Dirac-Brueckner predictions is both appropriate and timely.

Apart from the sizable 3BF enhancement of the repulsive component of the effective interaction (G matrix in Brueckner theory), the strong variation of the effective mass [9] is expected to impact the in-medium cross section via the level densities in the entrance and exit channels.

The potential used in our calculations is the Argonne v_{14} [27], which is modeled on the experimental phase shifts. The more general charge dependent Argonne v_{18} does not give appreciable variations.

Therefore the theoretical NN cross sections in free space are in excellent agreement with the experimental data, as shown in Fig. 5. There, we also show that the total cross sections, σ_{NN} and σ_{pn}, converge rapidly to the corresponding experimental values [28–31] with increasing number of partial waves. (Notice that in the DBHF predictions shown for comparison in Sec. IV C, the Bonn B potential is used [19]. This will be discussed below.)

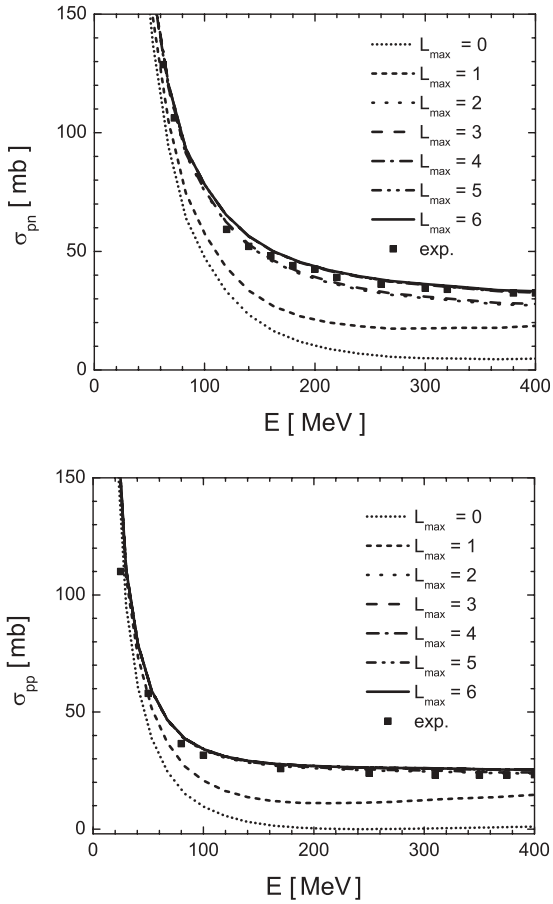

FIG. 5. Free-space pn and NN cross sections for increasing values of the maximum angular momentum and as a function of the incident laboratory energy, E. The squares represent the experimental data.

A. Identical particles

We examine three typical situations, i.e., low density ($\rho = 0.08$ fm^{-3}), saturation density ($\rho = 0.16$) and high density ($\rho = 0.35$). In Fig. 6, the in-medium cross sections from BHF calculations are displayed with and without three-body forces. The free cross section is also plotted for comparison. Up to the saturation density, the effect of the 3BF is small, and the medium suppression is mainly controlled by the reduction of density of states due to Pauli blocking. The asymptotic value is the same with and without the 3BF. At the higher density, the 3BF produces a larger reduction of the cross section, which persists up to high energy. The latter is mainly due to the strong 3BF renormalization of the effective mass shown in Fig. 2. In all calculations, the momentum dependence of the effective mass is taken into account, but the results do not change significantly if $m^*(k, k_F)$ is replaced by $m^*(k_F)$. The scattering amplitude is also affected by the 3BF, as shown in Fig. 1 for the $^1S_0$ partial wave, but it is difficult to disentangle the reduction of attractive two-body channels from the enhancement of the repulsive ones.

In Fig. 7, two sets of differential cross sections are displayed: $E = 100$ and $E = 240$ MeV. The curves are symmetric

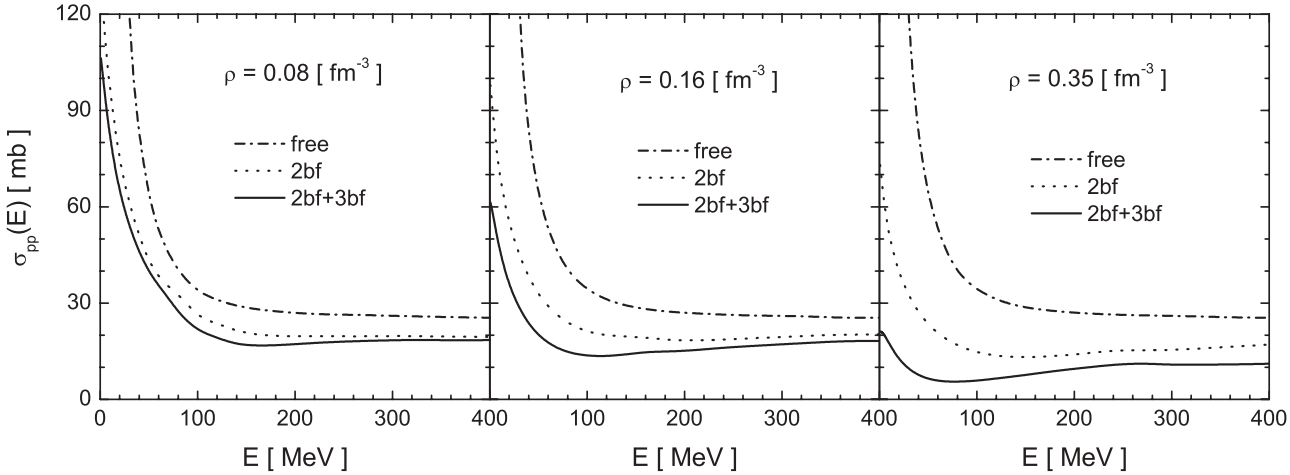

FIG. 6. Total cross sections for scattering of identical nucleons with and without the effect of 3BFs. The free-space cross section is shown for comparison.

around 90° (as they must be on fundamental principles), and bend up at forward and backward angles. The reduction of the cross section (present at all angles) is more sizable in the forward and backward directions, since low momentum transfers are strongly suppressed by the Pauli principle [5], as shown in Fig. 1. This effect leads to distributions that are almost flat at high density. This feature justifies the frequent practice of adopting isotropic cross sections in HIC simulations.

B. Nonidentical particles

In scattering of distinguishable nucleons, the $T = 0$ component of the interaction is also included. As a consequence, the free cross section for unlike particles is larger than the one for like particles, a property which remains true in the medium. The 3BF effect on the cross section is shown in Fig. 8. It is worth mentioning that the low-energy uprise of the in-medium σ_{pn} is a remnant of the pairing anomaly, which cannot be removed by hand at low density. The differential cross section $\sigma_{pn}(\theta)$ is strongly asymmetric. The in-medium values exhibit similar asymmetry although less pronounced (see Fig. 9).

C. Comparison with DBHF predictions

In this subsection, we compare the in-medium cross sections obtained with BHF+3BF as described above and the predictions of a recent DBHF calculation [25]. First, some technical remarks should be made. The effect of Pauli-blocking the final states (in addition to the intermediate states) was incorporated in the cross sections of Ref. [25]. That effect has been removed so as to make the predictions comparable with those presented in the previous subsections. Furthermore, unlike what was done in Ref. [25], all cross sections shown in this paper are calculated with the assumption that the nuclear matter rest frame and the center-of-mass frame of the two nucleons coincide.

In Tables II and III, q_0 is the momentum of either nucleon in its c.m. system, and the entries in the third column are the DBHF predictions for NN and np total cross sections, respectively. Our focal point is on the comparison between $\sigma_{NN/np}^{\mathrm{2BF+3BF}}$ and $\sigma_{NN/np}^{\mathrm{DBHF}}$.

First, we notice a generally fair agreement. For the np case, energy and density dependence appear quite consistent among the two sets of results, although $\sigma_{np}^{\mathrm{2BF+3BF}}$ is somewhat larger than $\sigma_{np}^{\mathrm{DBHF}}$ across the board. The $\sigma_{NN}^{\mathrm{DBHF}}$ values are in good

TABLE II. NN total effective cross sections (in mb) in symmetric matter calculated with various many-body models. The results shown in column 3 are obtained with Bonn B and the DBHF model.

$k_F(\mathrm{fm}^{-1})$	$q0$ (MeV)	$\sigma_{NN}^{\mathrm{DBHF}}$	$\sigma_{NN}^{\mathrm{2BF+3BF}}$	$\sigma_{NN}^{\mathrm{2BF}}$
1.1	250	18.00	18.15	22.98
1.1	300	16.41	17.47	19.48
1.1	350	17.08	18.55	19.51
1.4	250	15.72	13.74	19.76
1.4	300	13.70	14.43	17.23
1.4	350	16.31	16.89	19.46
1.7	250	18.05	7.87	13.36
1.7	300	17.93	9.98	13.98
1.7	350	13.96	11.48	16.43

TABLE III. Same as Table II, but for nonidentical particles.

$k_F(\mathrm{fm}^{-1})$	$q0$ (MeV)	$\sigma_{np}^{\mathrm{DBHF}}$	$\sigma_{np}^{\mathrm{2BF+3BF}}$	$\sigma_{np}^{\mathrm{2BF}}$
1.1	250	34.38	44.65	51.74
1.1	300	23.14	29.01	31.85
1.1	350	20.63	23.56	25.62
1.4	250	26.74	31.25	39.82
1.4	300	17.26	25.28	30.96
1.4	350	16.77	21.17	25.23
1.7	250	17.20	19.03	29.12
1.7	300	15.06	17.59	25.02
1.7	350	12.33	13.99	21.04

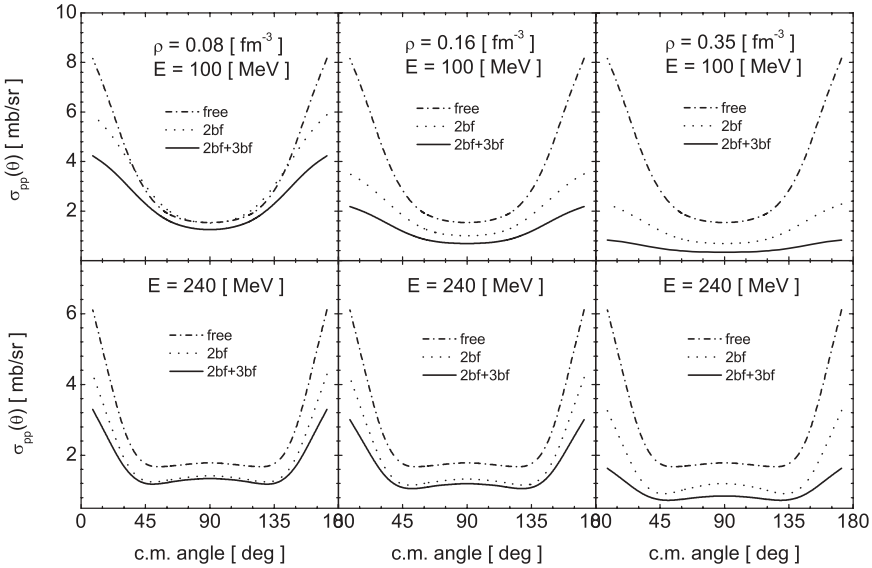

FIG. 7. Center-of-mass differential cross section for scattering of identical nucleons with and without the effect of 3BFs at $E =$ 100 and 240 MeV. The free-space cross section is also shown for comparison.

agreement with $\sigma_{NN}^{2BF+3BF}$, with the exception of the highest density.

The differences and/or similarities apparent from Table I can help shed light on the cross section comparison. The agreement is reasonable at low to moderate densities but deteriorates at $k_F = 1.7$ fm^{-1}, consistent with the large differences present at high density between the DBHF and the BHF+3BF predictions of the EOS. Examination of the last column in Table I clearly suggests that 3BFs other than Z diagrams are the main cause of the discrepancies between the DBHF and the BHF+3BF predictions of the EOS and, consequently, of the respective cross sections.

There are other possible sources of differences between the two models, which at this point we do not expect to have a dramatic impact on the present conclusions but which nevertheless will be explored more fully in a forthcoming work:

(1) Free-space models applied. The BHF+3BF calculation is presently not available with Bonn B. (Note that for a different two-body potential, 3BFs need to be reconstructed consistently with the parameters of that potential.) Therefore, the two sets of predictions we are comparing do not share exactly the same baseline. On the other hand, it is well known that the major source of model dependence among (*quantitative*) potentials is the off-shell behavior of the tensor force, which can impact in-medium properties (since the G matrix is obviously not constrained by two-body data). In the effort to gain some control over this uncertainty factor, we have examined DBHF predictions obtained with the Bonn A, B, and C potentials (the DBHF calculation is not feasible with Argonne v_{14}). This test should give us a realistic idea of the typical spreading of predictions with changing strength of the tensor force. A representative case is shown in Table IV. There, we see that the dependence on the potential model is moderate, although

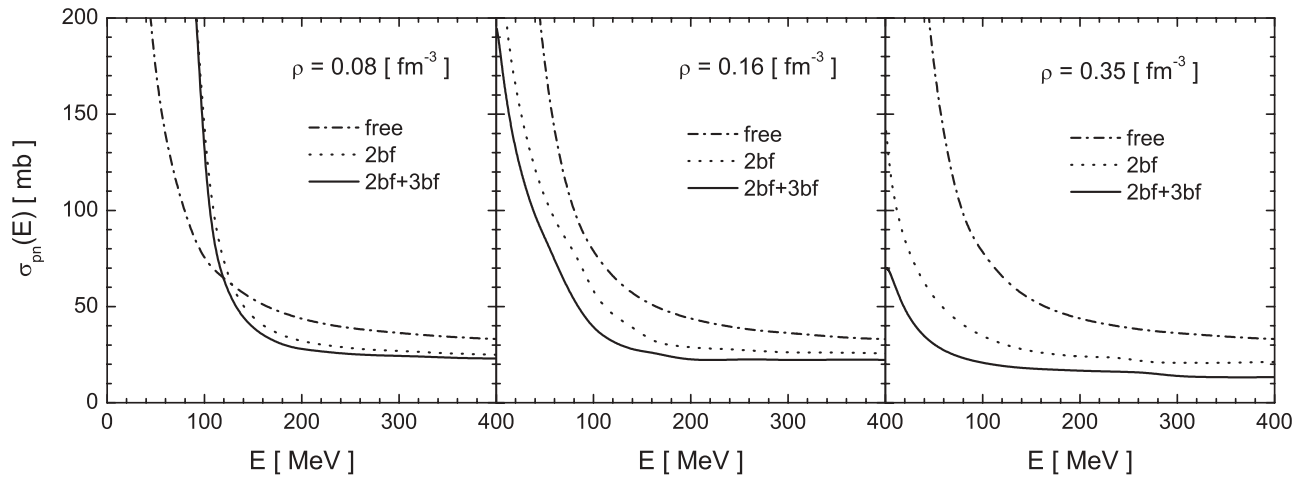

FIG. 8. Same as Fig. 6, but for nonidentical particles.

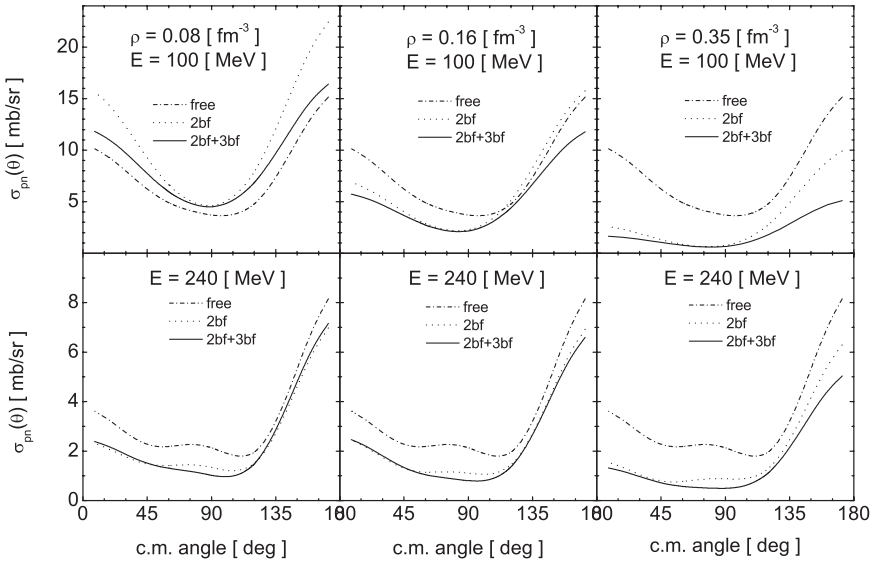

FIG. 9. Same as Fig. 7, but for nonidentical particles.

a bit more pronounced in the np channel, as to be expected. We conclude that the choice of the free-space model (provided it is quantitative in the description of two-body data) is not likely to be the major source of discrepancies. Nevertheless, in the near future, we hope to reconsider this comparison with the 3BF calculated with the same meson parameters as used in the DBHF calculation. This effort is in progress.

(2) Effective masses. Effective masses are essentially a byproduct of the self-consistent nuclear matter calculation. As such, they are the physical "link" between the calculation of nuclear matter saturation observables and the one of in-medium scattering properties. The value of the effective mass is, of course, closely related to the nature of the calculation (e.g., 2BF vs 3BF), but it also depends on various choices and approximations, not necessarily inherent to the issue at hand. An example is the momentum dependence. The masses displayed in Fig. 2 are density and momentum dependent, whereas those used in the DBHF calculations are only density dependent, due to the particular ansatz employed to fit the single-particle spectrum in the corresponding nuclear matter calculation. As mentioned in Sec. IV A, the BHF+3BF calculations were repeated using $m^*(k_F)$ at the appropriate density instead of $m^*(k, k_F)$, thus eliminating the momentum dependence, and the results were found to remain fairly stable. Lastly, we performed sensitivity tests where we used the same (momentum-independent) masses in both calculations (BHF+3BF and DBHF) and observed a systematic improvement in the agreement.

TABLE IV. Sample of potential model dependence of $\sigma_{NN}^{\mathrm{DBHF}}$ and $\sigma_{np}^{\mathrm{DBHF}}$ (in mb).

k_F (fm^{-1})	$q0$ (MeV)	Potential	$\sigma_{NN}^{\mathrm{DBHF}}$	$\sigma_{np}^{\mathrm{DBHF}}$
1.7	300	A	18.23	14.08
1.7	300	B	17.93	15.06
1.7	300	C	17.59	16.09

V. CONCLUSIONS

In this work, medium modifications on NN cross sections have been revisited within the BHF approximation including three-body forces. The inclusion of 3BF effects allows us to extend the range of validity of our predictions up to two to three times the saturation density. In this approximation, the scattering amplitude (G matrix) embodies not only the mean field dispersive effect and Pauli blocking but also a number of important medium modifications due to the virtual excitation of $N\bar{N}$ pairs and nucleon resonances [7]. The 3BF induces a stronger suppression of the total cross section for both NN and np scatterings. The main effect is the strong reduction of the density of states in the entrance and exit channels due to the rearrangement term in the self-energy, which can also be traced back to the 3BF. We have presented both total and differential cross sections. Concerning the latter, we observed a large 3BF suppression of the higher angular momenta leading to nearly isotropic distributions at high density. This feature partially supports the use of constant cross sections in the dynamical simulations of heavy-ion collisions.

An interesting point often discussed in the literature is the extent to which relativistic effects such as those characteristic of the DBHF approach are equivalent to (some) three-body forces, particularly those corresponding to virtual nucleon-antinucleon excitations. To pursue this line of investigation, we compared the 3BF-modified cross sections with those from recent DBHF calculations. Generally, we found a fair amount of agreement. We discussed similarities and differences and examined potential sources of model dependence. The comparison displayed in Table I indicates that the DBHF scheme is reasonably consistent with a nonrelativistic BHF model including Z-graph contributions.

To conclude, it has been known for a long time that a strongly density-dependent repulsive effect on the energy per nucleon in nuclear matter can be the result of relativistic effects as well as many-body forces. Nevertheless, there are still open questions which can now be investigated thoroughly as available many-body calculations become more and more sophisticated (with microscopic 3BFs consistently derived from 2BFs). Thus it becomes interesting and timely to revisit these issues.

ACKNOWLEDGMENTS

This work was supported by European Commission under Grant No. CN/ASIA-LINK/008(94791). F.S. acknowledges support by the U.S. Department of Energy.

[1] *Dynamics and Thermodynamics with Nuclear Degrees of Freedom*, Eur. Phys. J. A **30** III (2006), edited by P. Chomaz, F. Gulminelli, W. Trautmann, and S. J. Yennello (Springer-Verlag, Berlin, 2007).
[2] A. Bohnet, N. Ohtsuka, J. Aichelin, R. Linden, and A. Faessler, Nucl. Phys. **A494**, 349 (1989).
[3] H.-J. Schulze, A. Schnell, G. Röpke, and U. Lombardo, Phys. Rev. C **55**, 3006 (1997).
[4] G. Q. Li and R. Machleidt, Phys. Rev. C **48**, 1702 (1993); **49**, 566 (1994).
[5] C. Fuchs, A. Faessler, and M. El-Shabshiry, Phys. Rev. C **64**, 024003 (2001).
[6] V. R. Pandharipande and S. C. Pieper, Phys. Rev. C **45**, 791 (1992).
[7] P. Grange, A. Lejeune, M. Martzolff, and J. F. Mathiot, Phys. Rev. C **40**, 1040 (1989).
[8] A. Lejeune, U. Lombardo, and W. Zuo, Phys. Lett. **B477**, 45 (2000).
[9] W. Zuo, A. Lejeune, U. Lombardo, and J. F. Mathiot, Eur. Phys. J. A **14**, 469 (2002); Nucl. Phys. **A706**, 418 (2002).
[10] W. Zuo, U. Lombardo, H.-J. Schulze, and Z. H. Li, Phys. Rev. C **74**, 014317 (2006).
[11] G. E. Brown, W. Weise, G. Baym, and J. Speth, Comments Nucl. Part. Phys. **17**, 39 (1987).
[12] M. R. Anastasio, L. S. Celenza, W. S. Pong, and C. M. Shakin, Phys. Rep. **100**, 327 (1983).
[13] J. P. Jeukenne, A. Lejeune, and C. Mahaux, Phys. Rep. **25**, 83 (1976).
[14] W. Zuo, I. Bombaci, and U. Lombardo, Phys. Rev. C **60**, 024605 (1999).
[15] U. Lombardo, H.-J. Schulze, and W. Zuo, Phys. Rev. C **59**, 2927 (1999).
[16] A. Amorim and J. A. Tjon, Phys. Rev. Lett. **68**, 772 (1992).
[17] F. Gross, J. W. Van Orden, and K. Holinde, Phys. Rev. C **45**, 2094 (1992).
[18] F. de Jong and H. Lenske, Phys. Rev. C **58**, 890 (1998).
[19] R. Machleidt, Adv. Nucl. Phys. **19**, 189 (1989).
[20] F. Sammarruca, arXiv:0708.2112v1 [nucl-th].
[21] E. N. E. van Dalen, C. Fuchs, and A. Faessler, Phys. Rev. C **72**, 065803 (2005).
[22] G. Giansiracusa, U. Lombardo, and N. Sandulescu, Phys. Rev. C **53**, R1478 (1996).
[23] J. Diaz-Alonso and Lysiane Mornas, Nucl. Phys. **A629**, 679 (1998).
[24] B. A. Li and L. W. Chen, Phys. Rev. C **72**, 064611 (2005); B. A. Li, P. Danielewicz, and W. G. Lynch, Phys. Rev. C **71**, 054603 (2005).
[25] F. Sammarruca and P. Krastev, Phys. Rev. C **73**, 014001 (2006).
[26] W. Z. Jiang, B. A. Li, and L. W. Chen, talk given at the International Symposium on Exotic States of Nuclear Matter, Catania, Italy, June 11–15, 2007, arXiv:0708.2561v1 [nucl-th].
[27] R. B. Wiringa, R. A. Smith, and T. L. Ainsworth, Phys. Rev. C **29**, 1207 (1984).
[28] A. Bol, P. Devescovi, P. Leleux, P. Lipnik, P. Macq, and J. P. Meulders, Phys. Rev. C **32**, 623 (1985).
[29] V. Grundies *et al*., Phys. Lett. **B158**, 15 (1985).
[30] K. Chen *et al*., Phys. Rev. **166**, 949 (1968).
[31] J. W. Wilson and C. M. Costner, NASA TN D-8107, 1975 (unpublished).